eLife

Reviewed Preprint
v1 • May 26, 2026
Not revised

For correspondence:
hartmut.schmidt@medizin.uni-leipzig.de

* These authors contributed equally

Competing interests: No competing interests declared

Funding: See page 16

Reviewing editor: Annalisa Scimemi, University at Albany, State University of New York, United States

Loose coupling between Ca^{2+} channels and release sensors as a synaptic correlate of higher order brain function

Max Schwarze*, Grit Bornschein*, Antonia Brunner, Akanksha Arshia, Simone Brachtendorf, Hartmut Schmidt
Carl Ludwig Institute for Physiology, Medical Faculty, University of Leipzig, Leipzig, Germany

eLife Assessment

By using a combination of patch clamp recordings, calcium imaging and computer modeling, the authors analyze the spatial distribution of voltage gated calcium channels at glutamatergic synapses formed between layer 5 pyramidal neurons (L5PNs) and between layer 2/3 and L5PNs in the prefrontal cortex (PFC) and primary somatosensory cortex (S1); they conclude that the calcium channel-vesicle coupling is looser in the PFC compared to S1, although additional experiments are needed to determine how the distinct functional characteristics of these synapses in different brain regions might affect data interpretation. Overall, these findings are **important** because they have implications for shaping synaptic plasticity and neural circuit function across brain regions. They are **solid** because they are based on the use of a multi-pronged approach, although the presentation would benefit from stronger integration of the current findings with the existing literature and a more explicit discussion of potential limitations and confounding factors for data interpretation.

https://doi.org/10.7554/eLife.110314.1.sa4

Abstract

In the mature neocortex, functionally distinct areas are built by the same archetypes of neurons, but depending on the area, these neurons and their synapses are engaged in very different functions, ranging from lower order processing of sensory information to higher order associations and cognitive functions. We found significant differences in the functional presynaptic nanoarchitectures of the same types of pyramidal neuron synapses, depending on whether they are located in the prefrontal cortex (PFC) or in the primary somatosensory cortex (S1). Synapses in PFC operated with loose microdomain coupling as opposed to tight nanodomain coupling in S1. These differences were associated with significant differences in synaptic timing, efficacy and plasticity between areas. Our data suggest that the mature neocortex uses tuning of synaptic topographies to specialize seemingly identical types of neurons for their required function. They reveal microdomain coupling as a presynaptic structure-function correlate of higher order neocortical functions.

Introduction

The neo- or isocortex is a morphologically homogeneous brain region that covers highly diverse functions within its specialized areas, ranging from early sensory processing and motor control up to higher order associations, cognition and consciousness (Douglas and Martin, 2004; Harris and Shepherd, 2015). Notably, all of these diverse functions are executed by the same archetypes of neurons and synapses. However, depending on the area, they are engaged to different degrees in

lower or higher order processing. Whether area-specific functional differences in the mature neocortex are associated with or even arise from differences in the functional presynaptic nanoarchitecture of the same principal types of synapses is currently unclear.

At presynaptic active zones, the coupling distance between voltage-gated Ca^{2+} channels (VGCCs) and transmitter-filled synaptic vesicles (SVs) is a major determinant of key synaptic properties, including speed, efficacy and reliability of synaptic transmission (Rozov et al., 2001; Fedchyshyn and Wang, 2005; Bucurenciu et al., 2008; Baur et al., 2015; Bornschein et al., 2019a; Chen et al., 2024), and also short-term plasticity, although the latter can be obscured by vesicle replenishment (Miki et al., 2016; Doussau et al., 2017; Bornschein et al., 2019b; Lin et al., 2022). Studies at different synapses in different parts of the brain suggest that excitatory synapses engaged in reliable information transfer switch from loose microdomain to tight nanodomain coupling during development (Fedchyshyn and Wang, 2005; Baur et al., 2015; Nakamura et al., 2015; Bornschein et al., 2019a). This includes synapses between layer 5 pyramidal neurons (L5PNs) in the primary somatosensory cortex (S1), an area of early sensory processing (Bornschein et al., 2019a). On the other hand, loose microdomain coupling was found in the mature brain to date only at a highly plastic hippocampal synapse and has been suggested to provide a molecular framework for presynaptic plasticity (Vyleta and Jonas, 2014). However, if microdomain coupling also represents a synaptic correlate of higher order neocortical function or if it restricted to specific and highly plastic synapses in the hippocampus is currently unclear. Therefore, here we tested the hypothesis that loose microdomain coupling is the synaptic correlate of higher order functions of the mature neocortex, whereas tight nanodomain coupling is the synaptic correlate of earlier processing stages. Our data show that in the mature cortex the same types of pyramidal neuron synapses operate with loose microdomain coupling if they are located in the prefrontal cortex (PFC), whereas in S1 they operate with tight nanodomain coupling. Thus, our results corroborate the hypothesis and suggest microdomain coupling as a synaptic correlate of higher order function in the neocortex.

Results

Synaptic efficacy, reliability and short-term plasticity differ between PFC and S1

We focused on the lateral prefrontal cortex (PFC) and medial prefrontal cortex (mPFC) as areas of higher order processing and on primary somatosensory cortex (S1) as an area of lower order processing. Within these areas we investigated excitatory synapses between pyramidal neurons (PNs), which are the principal building blocks of the neocortex. We first analyzed the properties of synapses connecting neighboring layer 5 PNs (L5PNs) in mature PFC (P21-26) by performing paired whole-cell patch-clamp recordings and compared their properties to those we previously reported for the same synapses and age in S1 (Bornschein et al., 2019b; Bornschein et al., 2019a) (Figure 1A). We found that the efficacy of transmission, i.e. the size of a unitary EPSC evoked by a single action potential (Rozov et al., 2001), was significantly lower in PFC (8 pA, 5-15 pA) than in S1 (29 pA, 18-53 pA), whereas the synaptic failure rates were significantly higher in PFC (0.16, 0.08-0.28) than in S1 (0, 0-0.03; Figure 1B-D). In addition, we found that the synaptic delays (2.46 ms, 2.20-2.94 ms) as well as their standard deviation (SD_{Delay}: 0.60 ms, 0.49-0.81 ms) were significantly larger in PFC than in S1 (delay: 1.99 ms, 1.67-2.25 ms; SD_{Delay}: 0.24 ms, 1.14-0.37 ms; Figure 1E, F), indicating that transmitter release is less tightly coupled to the time of the action potential in PFC than in S1 (Bullmann et al., 2024). Together these data show that synaptic speed, efficacy and reliability during single action potentials are lower in PFC than at the same synapses in S1.

When pairs of action potentials were applied at high frequency (Figure 1G-I), differences in the synaptic success rates were associated with a significant difference in the paired pulse ratios (PPR) between PFC and S1. In PFC paired pulse facilitation (PPF, 1.18, 0.98-1.52) prevailed associated with increased success rates in the 2^{nd} pulse (1_x: 0.81, 0.73-0.91; x_1: 0.91, 0.82-0.97). In contrast, in S1 paired pulse depression (PPD, 0.78, 0.69-0.90) was found with high initial success rates (1_x:

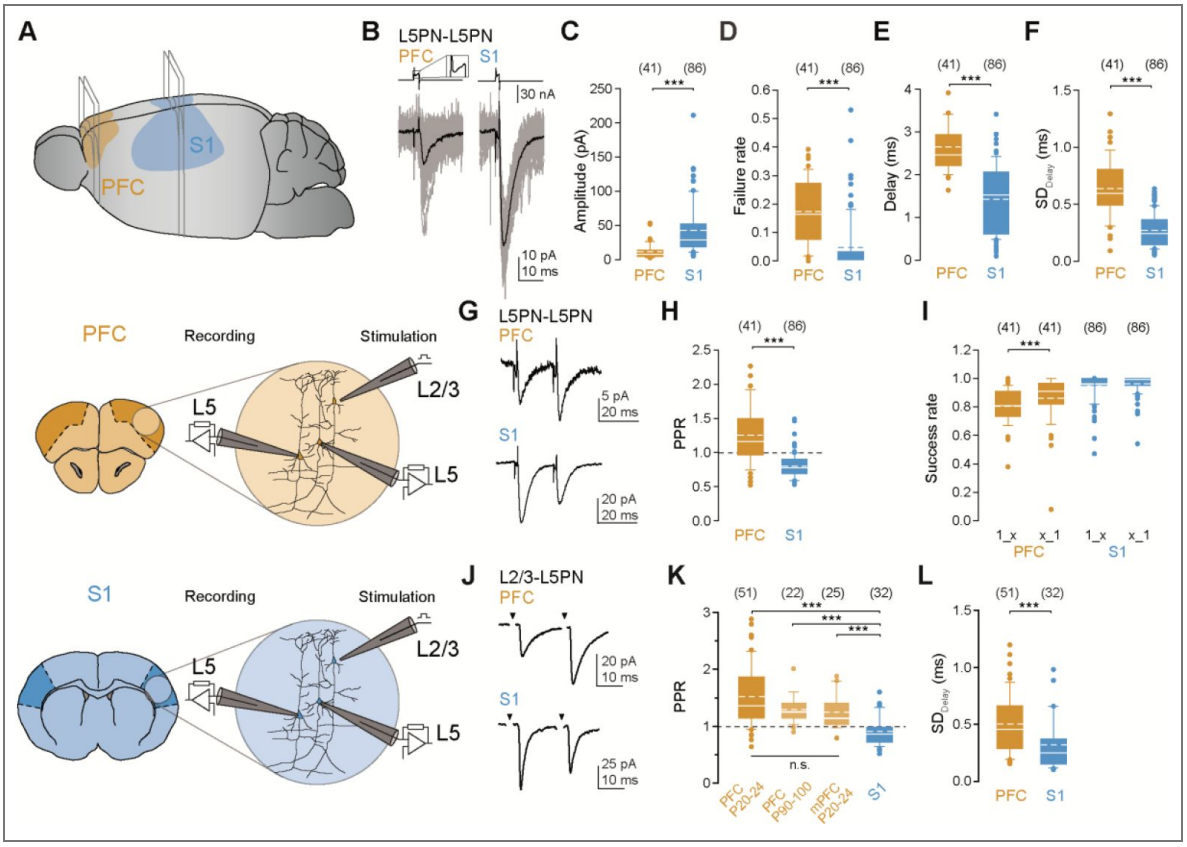

Figure 1. Differences in synaptic transmission and plasticity between PFC and S1 synapses.

(A) Schematic representation of the mature mouse brain (top) and the positions at which coronal sections were made from PFC (orange; middle) or S1 (blue; bottom). Recordings were made in acute slices from L5PN-L5PN pairs or from L2/3-L5PN connections. ***(B)*** EPSCs (bottom) recorded from postsynaptic L5PNs after evoking action currents in the presynaptic L5PNs (top, inset: 3fold magnification) in PFC (left) or S1 (right), individual recordings in gray, averages in black). ***(C-F)*** Summary of basic synaptic properties: EPSC amplitudes (***C***), failure rates (***D***), synaptic delays (***E***) and their SD values (***F***) in PFC and S1 (medians ± IQRs, means as dashed lines, whiskers represent 10th and 90th percentiles, dots indicate outliers, numbers of cell pairs in brackets; ***P<0.001, MWU). Data from S1 are from ref. (Bornschein et al., 2019a). ***(G)*** EPSCs recorded from pairs of L5PNs at 50 Hz intervals in PFC (top) and S1 (bottom), presynaptic stimulations are omitted, averages from at least 10 individual recordings). ***(H, I)*** Summary of PPRs (**H**; ***P<0.001, MWU) and success rates (**I**) following the 1st (1_x) and 2nd stimulation (x_1; ***P<0.001, P=0.987, WSR). S1 data are from ref. (Bornschein et al., 2019a). ***(J)*** As in (***G***) but for L2/3-L5 synapses (bottom, averages from at least 15 individual recordings, stimulation artefacts were blanked for clarity, arrowheads denote the time points of extracellular stimulation). ***(K)*** Boxplots summarizing PPR data from lateral PFC (PFC), medial PFC (mPFC), older PFC (P90-100) and in S1 (***P<0.001, MWU; n.s., not significant, P=0.067, ANOVA on ranks). ***(L)*** Comparison of SDs of the synaptic delays at L2/3-L5 synapses between PFC and S1 (***P<0.001, MWU).

1.00, 0.97-1.00; x_1: 0.99, 0.95-1.00). We observed the difference in short-term plasticity over a range of interstimulus intervals (ISIs) of 5 to 50 ms (*SI Appendix*, Figure S1A, B). Thus, the differences in synaptic efficacy and reliability between S1 and PFC during the first action potential correlate with differential short-term plasticity, with the emphasize in S1 being on the first transmission process while in PFC facilitation emphasized the subsequent release.

Next, we investigated transmission at synapses between L2/3 and L5PNs, using minimal extracellular stimulation near somata of L2/3PNs (Figure 1A). We found that also L2/3-L5PN synapses in PFC showed PPF (1.36, 1.14-1.88) as opposed to PPD in S1 (0.87, 0.72-0.99; Figure 1J, K). We observed this over a range of ISIs up to 100 ms (*SI Appendix*, Figure S1C, D). In addition, at PFC synapses the SD of the synaptic delays (0.46, 0.29-0.66) was again significantly larger than in S1 (0.25, 0.15-0.37; Figure 1L). Furthermore, we found larger EPSC decay time constants (τ_{decay}) in PFC compared to S1, possibly reflecting a contribution of different postsynaptic glutamate receptors (*SI Appendix*, Figure S2A, B). Indeed, application of the N-methyl-D-aspartate receptor (NMDAR) antagonist APV removed the difference in τ_{decay} between PFC and S1 (*SI Appendix*, Figure S2C-F). We extended the paired pulse experiments at L2/3-L5PN synapses in PFC to even older mice (P90-100) and to the mPFC (P21-26). We found that PPF persisted in the older age window (1.25, 1.14-1.41) and that also the synapses in mPFC showed PPF (1.14, 1.03-1.42; Figure 1K).

Together these results from glutamatergic synapses onto L5PNs show significant differences in the synaptic delays, efficacy, reliability and short-term plasticity between PFC and S1. The results would be consistent with area-specific differences in the functional coupling distances between VGCCs and SVs at the presynaptic active zones.

EGTA sensitivity of release is higher in PFC than in S1

To directly test for differences in the coupling distances, we investigated the sensitivity of release to synthetic Ca^{2+} chelators (Figure 2). The sensitivity of release to low millimolar concentrations of the kinetically slow Ca^{2+} chelator EGTA is a standard indicator of loose coupling (Eggermann et al., 2012). First, we performed recordings at pairs of L5PNs in mature PFC (Figure 2A, B). After 10 min of stable baseline recordings, the presynaptic neuron was patched a second time and equilibrated for 30 min with 10 mM EGTA-containing pipette solution. In these paired recordings we found a significant effect of EGTA onto release in PFC (0.67, 0.63-0.73; control: 1.02, 0.75-1.20). In identical experiments in S1, we had previously found release to be insensitive to the same concentration of EGTA (0.94, 0.71-1.02) (Bornschein et al., 2019a). These data provide evidence that the synapses between L5PNs in mature PFC do indeed operate with loose coupling, in contrast to their counterparts in S1.

We proceeded by comparing the EGTA sensitivity of release at L2/3-L5PN synapses between S1 and PFC, using extracellular stimulation and incubation with Ca^{2+} chelator-AM compounds (Figure 2C-F) (Baur et al., 2015; Kusch et al., 2018). Following 10 min of stable baseline recordings, slices were perfused with ACSF that either contained the DMSO/Pluronic containing solvent alone (control) or 10 µM of dissolved EGTA-AM or BAPTA-AM. The fast BAPTA interferes with release irrespective of the coupling topography, thereby, providing a positive control for the proper functioning of the AM-method (Eggermann et al., 2012). EPSC amplitudes were quantified during a subsequent 10 min period with perfusion with normal ACSF. During this test period, BAPTA significantly reduced EPSC amplitudes both in PFC (0.28, 0.12-0.32; control: 0.99, 0.84-1.02) and in S1 (0.08, 0-0.18; control: 0.85, 0.83-0.92). On the other hand, EGTA significantly reduced EPSC amplitudes only in PFC (0.57, 0.50-0.70; 58% of control) but not in S1 (0.85, 0.81-0.90; 100% of control).

In S1 we previously found that coupling switches from loose to tight during postnatal development between ~P10 and ~P20 (Bornschein et al., 2019a). To probe for a developmental retardation of this process in PFC, we extended the EGTA-AM experiments at L2/3-L5PN synapses to the older age-window of P90-100. Also, in these experiments we found a significant sensitivity of release to EGTA (0.76, 0.65-0.78; Figure 2D; *SI Appendix*, Figure S3*A*), indicating that loose coupling is a

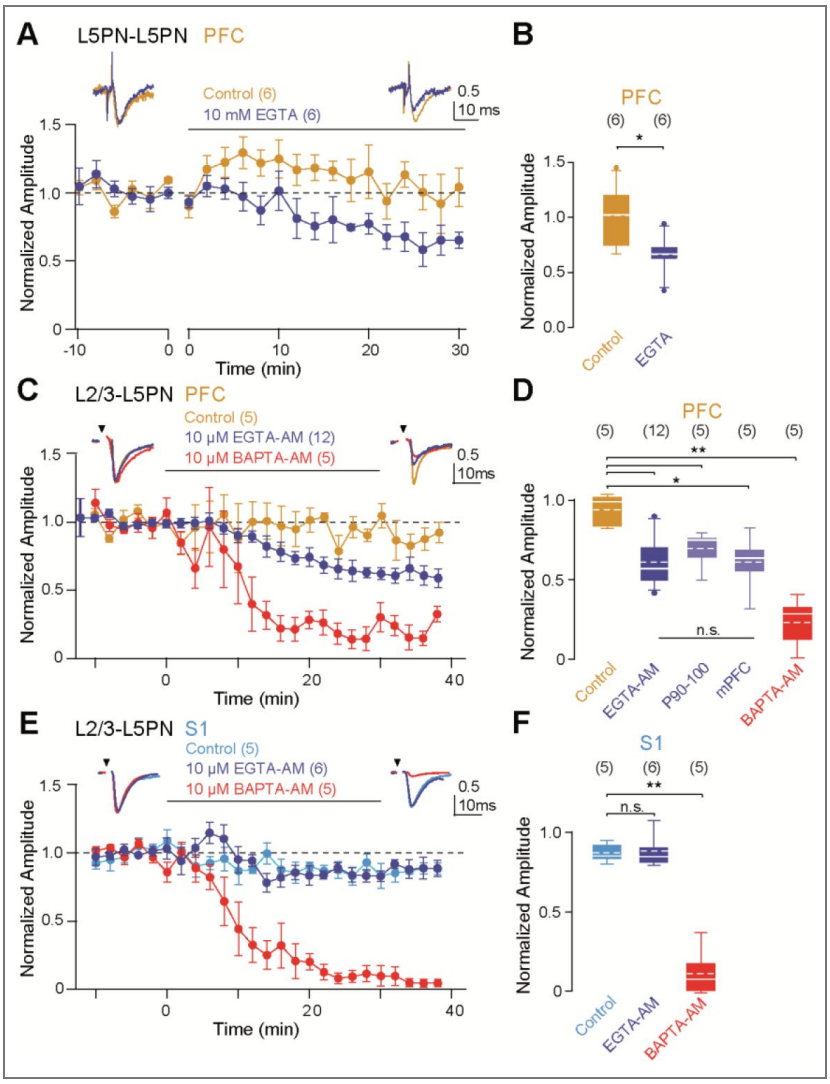

Figure 2. Area-specific differences in EGTA sensitivity.

(A) Averaged, baseline-normalized EPSC amplitudes (means ± SEMs, 2-min bins) recorded from L5PN-L5PN pairs in PFC with normal pipette solution (control, orange) and after re-patching the presynaptic neuron with a pipette solution containing 10 mM EGTA (blue). Insets: Average EPSCs from one pair during baseline (-10 to 0 min) and test period (20 to 30 min) for control and EGTA (averages normalized to baseline). ***(B)*** Boxplot comparing the normalized EPSC amplitudes prior and following the application of EGTA with control recordings in L5PN pairs in PFC (*P=0.041, MWU). Note the significant EGTA effect. ***(C)*** As in (***A***) but for L2/3-L5PN connections in PFC. Following baseline recordings (10 min), slices were perfused for 30 min (solid line) with ACSF containing either 10 µM EGTA-AM (blue), 10 µM BAPTA-AM (red), or only the solvent DMSO/Pluronic (control, orange), and thereafter rinsed for 10 min with ACSF (test period). Insets: Averaged EPSCs during baseline and test period. ***(D)*** Summary of chelator-AM effects in PFC, mPFC and older PFC (P90-100; *P=0.016, **P=0.007, 0.008, 0.008, MWU; P=0.404, ANOVA on ranks). Note the EGTA sensitivity of release in all PFC recordings. ***(E)*** As in (***C***) but for L2/3-L5PN connections in S1 (control in light blue). ***(F)*** Summary of chelator-AM effects in S1 (P=0.792, **P=0.008, MWU). Note the absence of a significant EGTA effect in S1.

functionally persistent feature of synapses in PFC. Finally, we also extended the EGTA-AM experiments to synapses in mPFC and again found significant effects of EGTA on the EPSC amplitudes (0.65, 0.49-0.75; Figure 2D; *SI Appendix*, Figure S3B).

Together the results obtained with the slow Ca^{2+} chelator EGTA suggest that major glutamatergic synapses in mature PFC operate with loose coupling in contrast to tight coupling in the mature S1. The data further suggest that loose coupling is a developmentally persistent property of synapses in PFC. Finally, they indicate that the above functional differences between synapses in S1 and PFC originate from the differences in Ca^{2+} influx-release coupling.

Release probabilities are similar in PFC and S1

To test whether the release probabilities (p_N) of the differentially coupled release sites in PFC and S1 differ, we performed multiple probability fluctuation analysis (MPFA) (Clements and Silver, 2000; Brachtendorf et al., 2025) at different extracellular Ca^{2+} concentrations ($[Ca^{2+}]_e$; Figure 3) (Bornschein et al., 2019a). The parabolic MPFA-fits to variance-mean plots from recordings of pairs of L5PNs in PFC yielded a median p_N of 0.50 (0.37-0.55; Figure 3A, D). This value was slightly but not significantly smaller than p_N of 0.66 (0.55-0.70), which we quantified previously for this connection in S1 (Bornschein et al., 2019a).

We also quantified p_N at L2/3-L5PN synapses, both in PFC and in S1, using MPFA with extracellular stimulation (Baur et al., 2015). We found that p_N was as high as at the L5PN-L5PN synapses in both areas with values (PFC: 0.62, 0.47-0.67; S1: 0.48, 0.39-0.58) being not significantly different between areas (Figure 3B, C, F). Interestingly, in our previous study (Bornschein et al., 2019a) we found that the developmental switch from loose to tight coupling at L5PN synapses in S1 also had no significant impact on p_N.

From MPFA in paired recordings it is possible to estimate the number of release sites (N) and the quantal size (q), additionally. N was significantly smaller in PFC than in S1 being only 2.1 (1.9-2.3) rather than 8 (3-19). q tended to be smaller in PFC (6 pA, 5-7 pA) than in S1 (9 pA; 8-11 pA) and the difference became significant when evoked quantal EPSCs recorded in low $[Ca^{2+}]_e$ were compared (PFC: 4 pA, 4-5 pA; S1: 9 pA, 7-11 pA). We consider it unlikely that postsynaptic receptor saturation or desensitization influenced the determination of quantal parameters since experiments with the competitive low-affinity glutamate receptor antagonist γ-DGG (γ-D-glutamylglycine) (Chanda and Xu-Friedman, 2010) performed at the S1 synapses had revealed no signs of this (p_N=0.58, 0.52-0.60; N=8, 8-12; Figure 3D). Due to the smaller size of the EPSCs, testing on the PFC synapses was not possible. Estimating EPSC amplitudes (EPSC = $N\ p_N\ q$; PFC, 6 pA; S1, 48 pA) and failure rates (F = $(1\text{-}p_N)\text{^}N$; PFC, 0.25, S1, 0.0001) from the quantal parameters yielded values that were well suited to explain the area-specific differences in synaptic efficacy during individual action potentials (Figure 1).

Presynaptic Ca^{2+} signals are similar in PFC and S1

For a thorough interpretation of the above results knowledge about the presynaptic Ca^{2+} dynamics in the different synapses is required. We performed dual-dye two-photon Ca^{2+} imaging (Sabatini et al., 2002) at presumed presynaptic boutons located on axon collaterals of L5PNs in PFC and in S1. We quantified single action potential-mediated elevations in green over red fluorescence signals (ΔG/R) that were converted to increases in intracellular calcium ($\Delta[Ca^{2+}]_i$) (Figure 4) (Bornschein et al., 2019a). We found that neither the Ca^{2+} transients nor the decay time constants were significantly different between the cortical areas (Figure 4A-F; PFC: G/R=0.25, 0.23-0.31; $\Delta[Ca^{2+}]_i$=279 nM, 244-453 nM; basal $[Ca^{2+}]_i$=30 nM, 21-34 nM; $\tau_{decay,1}$=9 ms, 6-19 ms; $\tau_{deay,2}$=91 ms, 75-120 ms; S1: G/R=0.29, 0.25-0.39; $\Delta[Ca^{2+}]_i$=238 nM, 208-303 nM; basal $[Ca^{2+}]_i$=22 nM, 13-38 nM; $\tau_{decay,1}$=9 ms, 3-15 ms; $\tau_{decay,2}$=86 ms, 63-212 ms). The similarity in the presynaptic Ca^{2+} transients of boutons in PFC and S1 suggests that differences in the presynaptic Ca^{2+} influx are unlikely to be the cause for the differential Ca^{2+} chelator effects. Rather, they support the view that these differences result from loose coupling in PFC and from tight coupling in S1.

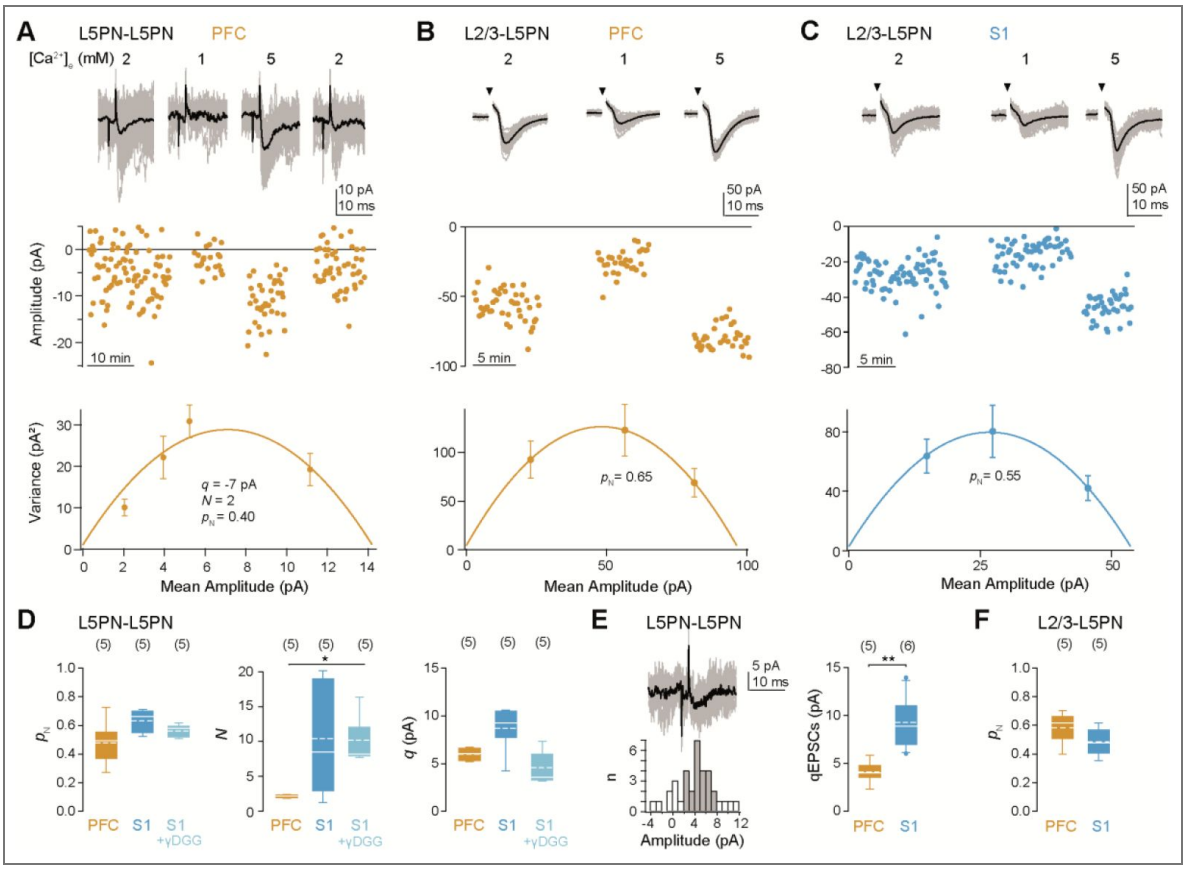

Figure 3. Quantal synaptic parameters in PFC and S1.

(A) MPFA of EPSC amplitudes recorded at the indicated $[Ca^{2+}]_e$ from a pair of L5PNs in PFC. Top: EPSCs (gray, average in black) recorded in 1, 2 and 5 mM $[Ca^{2+}]_e$. Middle: Plot of EPSC amplitudes over time. Bottom: Corresponding mean-variance plot fitted with a parabola estimating the quantal parameters of release. p_N is for 2 mM $[Ca^{2+}]_e$. ***(B)*** As in (***A***), but for a L2/3-L5PN connection in PFC. Recordings were made in the presence of 0.25 mM Kyn and 50 µM APV. ***(C)*** As in (***B***), but in S1. ***(D)*** Summary of quantal release parameters in L5PN pairs from PFC and S1 and in S1 with 1-2 mM γDGG (cf. (1); P=0.121, *P=0.048, ANOVA on ranks; P=0.054, MWU PFC vs. S1). ***(E)*** Left: Example of evoked qEPSCs (top) and the corresponding amplitude histogram (bottom, gray range was used for calculating the qEPSC amplitude). Right: Summary of qEPSC amplitudes in PFC and S1 (**P=0.004, MWU). ***(F)*** Summary of p_N values in L2/3-L5PN connections from PFC and S1 (P=0.222, MWU).

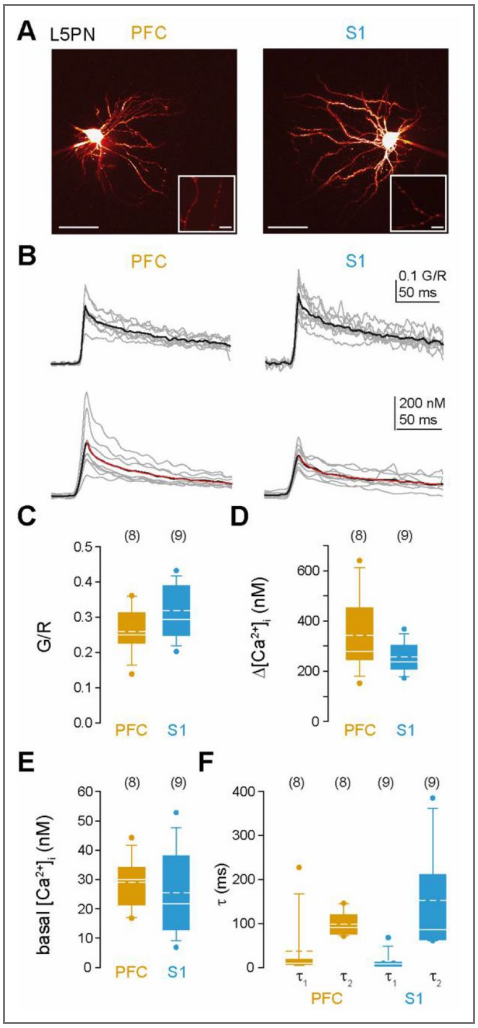

Figure 4. Presynaptic Ca^{2+} transients are similar in PFC and S1.

(A) Two-photon images of L5PNs in PFC (left) and S1 (right) filled with Fluo-5F and Alexa 594 (scale bar 50 µm). Insets: Magnifications showing presynaptic boutons from which Ca^{2+} transients are recorded (scale bar 5 µm). ***(B)*** G/R signals (top) evoked by single APs in individual cells (gray, average of 5-13 boutons each, grand average in black) and their conversion to Ca^{2+} increases ($\Delta[Ca^{2+}]_i$, bottom). ***(C-F)*** Summary of G/R signals (***C***; P=0.112, MWU), $\Delta[Ca^{2+}]_i$ (***D***; P=0.361), basal $\Delta[Ca^{2+}]_i$ (***E***; P=0.597) and decay time constants τ_1 and τ_2 (***F***; P=0.532, 0.962) in PFC and S1. Note, that there is no significant difference in presynaptic Ca^{2+} transients between PFC and S1.

Estimate of the coupling distance in PFC verify loose microdomain coupling in PFC

To derive a quantitative picture of the coupling topography in L5PN synapses in PFC we used numerical computer simulations that were based on and constrained by the experimental data. First, we simulated the measured Ca^{2+} transient with the indicator dye present in the simulation (Figure 5A). Subsequently, the indicator dye was removed and a release sensor model for Synaptotagmin-1-triggered release from L5PN boutons was included in the simulations (Figure 5B, C; *SI Appendix*, Figure S4) (Bornschein et al., 2025). VGCCs were assumed to form a ring like structure around a vesicle (Figure 5D), similar to the release site topography in young S1 (Bornschein et al., 2019a). Release rates as reported by the sensor model were integrated over time to yield the p_N values. The coupling distance between the sensor and the ring of VGCCs as well as the number of VGCCs forming the ring were iteratively varied until the simulation correctly predicted the experimental p_N values from MPFA obtained under control conditions and in the presence of EGTA. By this procedure we quantified an average coupling distance of 48-51 nm between a microdomain of several VGCCs and the release sensor (Figure 5B; *SI Appendix*, Figure S4), similar to the estimate for these synapses in immature S1 (Bornschein et al., 2019a). Thus, a microdomain model similar to immature S1 is suitable to predict the data from mature PFC, whereas the same synapses in mature S1 operated with Ca^{2+} signaling nanodomains in which only 1-3 VGCCs at distances of 11-16 nm trigger fusion (Bornschein et al., 2019a; Bornschein et al., 2025).

To experimentally test whether overlapping Ca^{2+} domains from several VGCCs trigger release in PFC (microdomain), we analyzed the effects of the unspecific VGCC blocker Cd^{2+} onto the PPR. If fusion is triggered by such VGCC microdomains, application of a subsaturating concentration of Cd^{2+} will increase the PPR, while it will leave PPR unaffected if only a single or few VGCCs trigger release (Hefft et al., 2002; Bucurenciu et al., 2008; Scimemi and Diamond, 2012; Baur et al., 2015; Bornschein et al., 2019a). In paired pulse experiments, at L2/3-L5PN synapses in PFC we indeed found a significant increase in the PPR following the application of 5 µM Cd^{2+} (rPPR=1.20±0.06), whereas the average PPR remained unaffected in S1 (rPPR=1.01±0.10; Figure 5E, F). Thus, our data and simulations suggest that the nanotopography of PN synapses in mature PFC is reminiscent of the same synapses in young S1.

Discussion

Our results provide evidence that the same archetypes of glutamatergic synapses show area-specific differences in their functional release site nanoarchitectures in the mature neocortex. They suggest loose microdomain coupling as a synaptic correlate of higher order neocortical functions.

The differences in coupling gave rise to larger synaptic delays in PFC compared to S1 and were associated with differences in synaptic reliability and efficacy, whereas the p_N values were not significantly different between areas. A major determinant of p_N is the size of the Ca^{2+} signal at the release sensor. Accordingly, tightening of coupling can increase p_N (Eggermann et al., 2012; Baur et al., 2015; Bornschein and Schmidt, 2019). However, large Ca^{2+} elevations at the release sensor can also be obtained with Ca^{2+} microdomains. At L5PN-L5PN synapses in S1 the developmental switch from microdomain to nanodomain coupling had no effect on p_N (Bornschein et al., 2019a). At the calyx of Held (Iwasaki and Takahashi, 2001; Taschenberger et al., 2002; Fedchyshyn and Wang, 2005; Koike-Tani et al., 2008; Nakamura et al., 2015) and at cerebellar basket cell to Purkinje cell synapses (Chen et al., 2024) p_N even decreased during development, whereas coupling got tightened. The decrease in p_N was compensated by an increase in N at these synapses, which increased their reliability and efficacy during development. We found N to be larger in S1 than in PFC. Thus, it appears that differences in coupling are typically associated with other characteristic changes in the release parameters. Overall, this suggests that

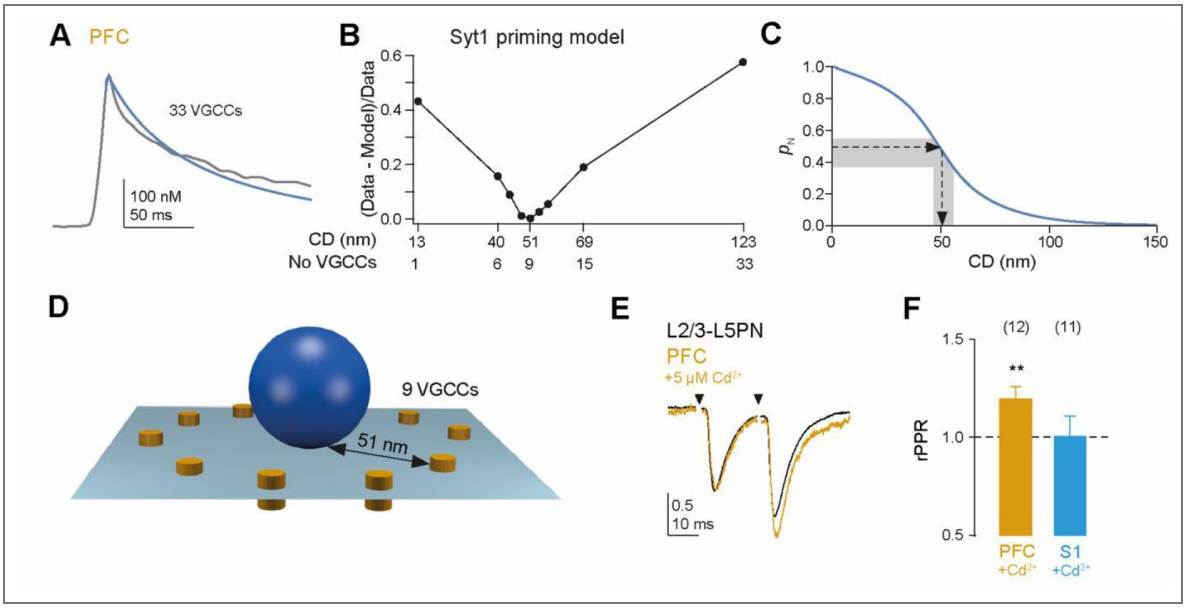

Figure 5. Model predicts microdomain coupling at PFC synapses.

(A) Fit of the model (blue line) to the measured average Ca^{2+} signal (***A***; gray line) of L5PN boutons in PFC. The fit was obtained with the indicated number of open VGCCs. ***(B)*** p_N values were simulated with the Syt1 priming model (Bornschein et al., 2019a; Bornschein et al., 2025) for control conditions and in the presence of EGTA with different VGCC numbers yielded different coupling distances (CD) in the model. The simulated p_N were subtracted from and normalized to the experimental values, i.e. a value close to zero indicates best agreement between simulation and experiment. This was obtained with 9 open VGCCs at a CD of 51 nm (see **C**). ***(C)*** Simulated p_N for 9 open VGCCs under control conditions at increasing CDs (blue line). The experimental p_N value (median ± IQR, dashed line, gray range, Figure 3D) was reproduced at a CD of 51 nm (48-55 nm). ***(D)*** Illustration of the ring model used in **B** and **C** with a CD of 51 nm between 9 VGCCs (orange) and the release sensor of a vesicle (blue). ***(E)*** Examples of averaged normalized paired pulse recordings at 50 Hz at L2/3-L5PN synapses before (black) and after (orange) application of 5 µM Cd^{2+} in PFC. ***(F)*** Bar graph quantifying normalized PPRs after Cd^{2+} application in PFC and S1 (**P=0.005, P=0.667, paired t-Test). Note that Cd^{2+} increased the PPR in PFC.

reliable synapses switch from an initial state with high plasticity to a matured state with high reliability. On the other hand, PN synapses in the PFC appear to remain in a more juvenile state that favors plasticity over reliability.

We observed differences in short-term plasticity that suggest that S1 emphasized the first transmission process, whereas in PFC facilitation emphasized the subsequent release. The mechanisms of short-term plasticity are complex and include the regulation of p_N, the speed of vesicle replenishment and the recruitment of release sites (Neher and Brose, 2018; Schmidt, 2019; Neher, 2023; Brachtendorf et al., 2025). We consider the differential emphasize on the available presynaptic efficacy between PFC and S1 as a signature of higher plasticity and flexibility in the processing of information in PFC compared to S1.

Our results have implications for long-term plasticity at neocortical PN synapses. Both, long-term potentiation (LTP) and depression (LTD) have a presynaptic locus at these synapses and likely involve changes in p_N, but the final steps that alter release are not well understood (Feldman, 2009; Castillo, 2012; Feldman, 2012). A recent study on L5PN synapses in S1 showed an increase in the number of primed vesicles as a major mechanism of LTP (Weichard et al., 2023). PN synapses in S1 are already tightly coupled and therefore a further decrease in the coupling distance is an unlikely mechanism of LTP. However, this does not exclude that in S1 LTD induction breaks tight coupling and vice versa that LTP in PFC involves tightening of coupling. In addition, in PFC we found an increased contribution of NMDAR on the postsynaptic site. Thus, these synapses have increased potential for plasticity on the pre- and the postsynaptic site. During induction of long-term plasticity, the postsynaptic site signals back to the presynaptic site via retrograde messengers (Regehr et al., 2009) and loose coupling will provide the substrate for enhanced regulatory capacity (Vyleta and Jonas, 2014).

In general, loose coupling provides more flexibility to regulate $[Ca^{2+}]_i$ at the release sensor (Vyleta and Jonas, 2014). Prefrontal networks carry out higher-order computations that transform sensory information and memory to perform flexible output such as delayed response, inference and planning (Narayanan et al., 2025). Our findings suggest that loose coupling provides a synaptic foundation for such flexible neocortical network functions.

Methods

Slice preparation

C57BL/6J mice at P21-26 of either sex were used in this study. All experiments were performed in accordance with the guidelines for the welfare of experimental animals issued by the European Communities Council Directive (2010/63/EU) and with the German Protection of Animals Act (Tierschutzgesetz). Mice were bred in the animal facility of the Medical Faculty of Leipzig University and were housed in individually ventilated cages in a specific pathogen free environment and in a 12h/12h light dark cycle with access to food and water ad libitum. Experiments were approved by the animal welfare office of the University Medical Center, Leipzig, as well as the local governmental authorities (Landesdirektion Leipzig, registration numbers T10/20, T05/21-MEZ).

C57BL/6J mice at P21-26 of either sex were decapitated under deep Isoflurane (Curamed) inhalation anesthesia. The brain was excised rapidly and placed in cooled (0-4°C) artificial cerebrospinal fluid (ACSF) containing (in mM): 125 NaCl, 2.5 KCl, 1.25 NaH_2PO_4, 26 $NaHCO_3$, 1 $MgCl_2$, 2 $CaCl_2$, and 20 glucose, equilibrated with 95% O_2 and 5% CO_2 (pH 7.3-7.4). Coronar neocortical slices (150-250 µm thick) were cut from the PFC or S1 region (Figure 1A) with a vibratome (HM 650 V, Microm). For some paired recordings between L5PNs and for calcium imaging experiments parasagittal slices (200 µm) were prepared from PFC region. Slices were incubated for 30 min at 35°C and subsequently stored at room temperature. For experiments, slices were transferred to a recording chamber and continuously perfused with ACSF (2-3 ml per min, supplemented with 10 µM (-)-bicuculline methiodide (Tocris) at 31-33°C. Unless stated otherwise, chemicals were from Sigma-Aldrich.

Electrophysiological recordings

Patch-clamp recordings from L5PNs were established as described in detail previously (Bornschein et al., 2019a; Bornschein et al., 2025). Patch pipettes were prepared from borosilicate glass (Hilgenberg) with a PC-10 puller (Narishige) and had final resistances of 6-8 MΩ when filled with the following standard pipette solution (in mM): 150 K-gluconate, 4 NaCl, 3 $MgCl_2$, 3 Na_2ATP, 0.3 NaGTP, 0.05 EGTA, 10 KHEPES, dissolved in purified water. The pH was adjusted to 7.3 with KOH. Recordings were performed under optical control (BX51WI, Olympus), using an EPC10/2 amplifier and Patchmaster software (version v2x90.2, HEKA). EPSCs were recorded in the whole-cell configuration at a holding potential (V_{hold}) of -90 mV (online corrected for a liquid junction potential of 16 mV), filtered at 5 kHz and sampled at 10 kHz. Series resistance (R_s) was continuously compensated to a fixed value between 10 and 15 MΩ. The average uncompensated R_s was 18±1 MΩ in L5PN-L5PN paired recordings (n=41 cells, mean ± SEM) and 23±1 MΩ in L2/3-L5PN recordings (n=133 cells). Holding current (I_{hold}) was also monitored continuously and was <180 pA (-134±16 pA in L5PN-L5PNs; -168±11 in L2/3-L5PNs). Presynaptic L5PNs were stimulated in on-cell configuration (200-500 mV, 1-2 ms).

For chelator wash-in experiments, presynaptic neurons were stimulated in the whole-cell configuration after re-patching with a pipette solution supplemented with 10 mM EGTA (K-gluconate concentration was reduced to 135 mM to adjust osmolarity). EPSCs were evoked every 10 s for at least 30 min (Figure 2). Averaged EPSC amplitudes were calculated before (≥10 min baseline) and 20-30 min after repatching (test period). For recordings from L2/3-L5PN connections ACSF-filled patch pipettes were placed close to the somata of PNs in L2/3 and extracellular stimulation was performed using an ISO-Stim 01 DPI (NPI electronics). Minimal stimulation (0.5 to 5 V) was used and yielded EPSC amplitudes of ~40 pA (47±3 pA, n=131 pairs), making it likely that we investigated transmission mainly between single or few L2/3PNs and L5PNs in these experiments. Following 10 min of stable recordings in normal ACSF (baseline), the bath solution was exchanged for ACSF containing either 0.1% DMSO and 0.01% Pluronic (control solution), 10 µM EGTA-AM or 10 µM BAPTA-AM in DMSO/Pluronic for 30 min (incubation period) and thereafter replaced by normal ACSF again for another 10 min (test period). Averaged EPSC amplitudes were calculated during baseline and test period. The time courses of chelator effects on EPSC amplitudes were analyzed by binning EPSC amplitudes within 2 min intervals of recording time to average amplitudes. Chelator effects were expressed as averaged EPSC amplitudes during test period normalized to the corresponding baseline values.

VGCCs were inhibited by bath-application of ACSF containing a subsaturating concentration of 5 µM $CdCl_2$ (Figure 4J). NMDA receptors were blocked by the selective antagonist 2-Amino-5-phosphonovaleriansäure (APV, 50 µM; *SI Appendix*, Figure S2). For assessing the effects of the individual blockers, EPSCs were recorded in ACSF for at least 10 min (10 s intervals), subsequently the blocker was perfused and the blocker effects were quantified after a stable block had been established (at least 5 min test period).

Quantification of quantal synaptic parameters

Quantal synaptic parameters were estimated from parabolic fits to mean-variance (MV) plots of EPSC amplitudes recorded at different $[Ca^{2+}]_e$ (1, 2, and 5 mM, ≥30 repetitions per concentration; $[Mg^{2+}]_e$ was correspondingly adjusted to 2, 1, 0 mM, respectively), assuming binominal release statistics (Clements and Silver, 2000; Scheuss et al., 2002; Silver, 2003). The recordings always started in 2 mM $[Ca^{2+}]_e$. The variance of EPSCs (σ^2) was calculated according to ref. (Scheuss et al., 2002), plotted against the averaged amplitudes (I), and fitted by a parabola of the form:

$$\sigma^2 = Iq - \frac{I^2}{N}\left(1 + CV_{II}^2\right) + qICV_1^2 \quad (1)$$

where q is the quantal size, N a binominal parameter, and CV_I and CV_{II} the coefficients of intrasite and intersite quantal variability, assumed to be 0.3 (Clements and Silver, 2000). The fits were constrained to pass through zero. The variance of the variance was calculated according to ref. (Meyer et al., 2001). Stationarity of EPSC amplitudes was established

when, after full exchange of the bathing solutions (≥5 min), EPSC amplitudes no longer showed a tendency to increase or decline. For MV analysis in L2/3- L5PN connections, the bath solution was supplemented with the competitive AMPA receptor antagonist kynurenic acid (Kyn, 0.25 mM), which relieves their desensitization and saturation (Neher and Sakaba, 2001) and with 50 µM APV to prevent NMDAR activation (Figure 3). Due to the small size of EPSCs in L5PN-L5PN connections no blocker was used in these recordings. The size of qEPSCs was quantified from evoked miniature EPSCs recorded in low $[Ca^{2+}]_e$ (1 mM) and high $[Mg^{2+}]_e$ (2 mM).

Ca^{2+} imaging

Action potential-evoked (current injection of 1-4 nA for 1-2 ms) fluorescence changes were recorded at boutons located on axon collaterals of L5PNs as described previously (Bornschein et al., 2019a; Bornschein et al., 2025). L5PNs were filled with EGTA-free, Fluo-5F (200 µM, Invitrogen) and Alexa-594 (50 µM, Molecular Probes) containing pipette solution via somatic whole-cell patch-pipettes. Cells were dialyzed for at least 20 min to yield sufficient equilibration with the dyes. Volume averaged fluorescence signals were recorded in point mode at 500 kHz temporal resolution and subsequently binned to 500 Hz, using a custom-build two-photon microscope based on a Fluoview-300 scanner (Olympus), a 60x/0.9

N.A. objective, a mode-locked Ti:sapphire laser (Tsunami, Newport-Spectra Physics, set to a center wavelength of 810 nm), and a Pockels cell (350-80 KD*P, Conoptics). The fluorescence background was determined in a subsequent point mode recording performed near the boutons under investigation. Typically, at least 5 boutons per L5PN were recorded and averages per cell were calculated. The fluorescence signals were filtered (HC647/75, Semrock HC525/50, 720-SP, AHF), detected by two external PMT modules (H7422-40, Hamamatsu; PMT-02M/PMM-03, NPI electronics) monitoring red and green epifluorescence, respectively at fixed PMT voltages, and digitized with the Fluoview system. The Ca^{2+}-dependent green fluorescence was normalized to the Ca^{2+}-insensitive red fluorescence and expressed as background-corrected ΔG/R (Sabatini et al., 2002). ΔG/R signals were converted to changes in $[Ca^{2+}]_i$ based on an *in vitro* quantification of the K_D of Fluo-5F (439 nM) in our pipette solution, adjusted with CaEGTA and K_2EGTA (100 mM stock solutions, 10 mM HEPES added) to contain different free Ca^{2+} concentrations that were calculated with the MaxChelator (*https://somapp.ucdmc.ucdavis.edu/pharmacology/bers/maxchelator/CaMgATPEGTA-NIST.htm*). R_{min} and R_{max} values were measured after each successful recording in sealed patch pipettes that were placed in the slices near the recorded cells. The pipettes contained the EGTA-free, Fluo-5F- and Alexa-594-containing pipette solution with either 0 mM $CaCl_2$ and 10 mM K_2EGTA (zero Ca^{2+} solution) or 20 mM $CaCl_2$ (high Ca^{2+} solution).

Modeling

The kinetic gating scheme of the VGCCs and the reaction schemes for Ca^{2+} binding to buffers and transmitter release were converted to ordinary differential equations (ODEs). The system of ODEs was numerically solved using “NDSolve” or “NDSolveValue” of Mathematica 14 (Wolfram) as described previously (Schmidt et al., 2013; Bornschein et al., 2019a; Bornschein et al., 2025). Spatial resolution was achieved by placing the ODEs in concentric hemi-shells (1 or 2 nm thickness) that were coupled via diffusion.

The presynaptic action potential was modeled with a half-duration of 0.2 ms, τ_{rise} of 0.1 and τ_{decay} of 0.2 ms (Borst et al., 1995). Voltage dependent activation of VGCCs was simulated using the gating scheme for P/Q-type channels, a single channel conductance of 2.5 pS, and a Ca^{2+} equilibrium potential of 130 mV (Li et al., 2007). The model included ATP as mobile buffer and immobile endogenous buffers with a buffer capacity (κ_E) of 25 (Tran and Stricker, 2018). Model parameters are given in Table S1 (*SI Appendix*).

The model for each channel consisted of five closed (C) and one open (O) state. The transition between the first five steps was voltage dependent and the last step voltage independent:

$$C_0 \underset{\beta_1(V)}{\overset{\alpha_1(V)}{\rightleftarrows}} C_1 \underset{\beta_2(V)}{\overset{\alpha_2(V)}{\rightleftarrows}} C_2 \underset{\beta_3(V)}{\overset{\alpha_3(V)}{\rightleftarrows}} C_3 \underset{\beta_4(V)}{\overset{\alpha_4(V)}{\rightleftarrows}} C_4 \underset{b}{\overset{a}{\rightleftarrows}} 0 \tag{2}$$

a and b are the rate constants for transitions between C_4 and O, and $\alpha_i(V)$ and $\beta_i(V)$ are the voltage dependent forward and backward transition rates that are given by:

$$\alpha_i(V) = \alpha_{i,0} \exp\left(V/k_i\right) \quad \mathrm{i} = 1-4 \tag{3a}$$

$$\beta_i(V) = \beta_{i,0} \exp\left(-V/k_j\right) \quad \mathrm{i} = 1-4 \tag{3b}$$

where $\alpha_{i,0}$ and $\beta_{i,0}$ are the forward and backward rate constants at 0 mV and k_i a slope factor.

Ca^{2+} binding to all buffers *(B)* was simulated by second order kinetics with forward and backward binding rate constants k_{on} and k_{off}, respectively:

$$\frac{d[Ca]}{dt} = -k_{on}[Ca][B] + k_{off}[CaB] \tag{4a}$$

$$\frac{d[B]}{dt} = -\frac{d[\mathrm{CaB}]}{dt} \tag{4b}$$

Diffusion of all species (X) was simulated according to

$$\frac{d[X]}{dt} = D_x \frac{A_{n,n\pm1}}{V_n r}\left([X]_{n\pm1} - [X]_n\right) \tag{5}$$

where D_X is the diffusion coefficient, A the surface, V the volume and r the radius of a shell (n). Ca^{2+} was cleared by a linear, surface-based extrusion mechanism driven by the difference between $[Ca^{2+}]_i$ and the resting $[Ca^{2+}]_i$ (30 nM according to the imaging data).

For fitting the model to the average experimental Ca^{2+} transient, the number of VGCCs was adjusted, yielding 33 VGCCs (Figure 4F). The other free parameter of the simulation was the extrusion rate, which however affected only the later phase of the decay of the transient. During fitting, the model included the Ca^{2+} indicator dye. Fitting was first performed in a single compartment model (Helmchen and Tank, 2005). Subsequently, fitting was performed in the spatially resolved model with the numbers of VGCCs remaining unaltered and $[Ca^{2+}]_i$ as reported by the dye was calculated from the concentration of the Ca^{2+}- dye complex assuming equilibrium conditions (Schmidt et al., 2003). Since L5PNs are characterized by an immobile and small κ_E with unknown binding kinetics, a slow (EB_s) and a fast immobile endogenous buffer (EB_f) were assumed (Helmchen et al., 1996; Ohana and Sakmann, 1998; Tran and Stricker, 2018). The fractions of EB_s and EB_f were adjusted to optimize the fit to the measured Ca^{2+} transient and to sum up to κ_E of 25. Following fitting, the indicator dye was removed from the model and the recently developed model for release from L5PN terminals was included (Bornschein et al., 2025). Either the “Syt1 priming model” (Equation 6; Figure 4) or the “Syt1 model” (Equation 7; *SI Appendix*, Figure S4) were placed at varying distances from the Ca^{2+} sources.

$$\frac{(Ca^{2+})^n}{(Ca^{2+})^n + K_M^n}\ R \xrightarrow{k_{prim}} V \underset{k_{off}}{\overset{Ca^{2+}\ 5k_{on}}{\rightleftharpoons}} CaV \ldots Ca_4V \underset{5k_{off}}{\overset{Ca^{2+}\ 4k_{on}}{\rightleftharpoons}} Ca_5V \rightarrow \mathrm{Fusion} \tag{6}$$

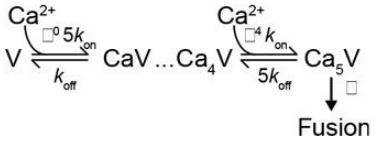

(7)

In the priming model (Equation 6), a single Ca^{2+}-dependent priming step with Michaelis-Menten kinetics (K_M) and a priming rate k_{prim} is assumed. V is the vesicular release sensor of a primed vesicle (Equation 6, 7) that binds a maximum of 5 Ca^{2+} ions. k_{on} and k_{off} are the forward and backward Ca^{2+} binding rate constants, β^i (i=0-4) is a cooperativity factor, and γ the fusion rate. p_N was obtained by integrating the release rates over time.

A ring like arrangement of the VGCCs around a vesicle was assumed (Figure 4I; ring 1 model in ref. (Bornschein et al., 2019a)). The number of VGCCs driving release was continuously reduced from the maximal value of 33 (Figure 4F) and the coupling distances at which the simulated p_N values matched the experimentally determined p_N were obtained. Subsequently, EGTA was included and the consistency between the experimentally quantified EGTA effect and the simulated EGTA effect at a given coupling distance was determined (Figure 4G). The best match between experiments and simulation was obtained for 9 VGCCs at a coupling distance of 51 nm (Figure 4H).

Quantification and statistical analysis

Data from L5PN-L5PN pairs in PFC were compared to previously published data from these pairs in S1 (Bornschein et al., 2019b; Bornschein et al., 2019a). Electrophysiological data and Ca^{2+} imaging data were analyzed using custom written routines in Igor Pro (version 6.32 and 8.03, Wavemetrics). Data are shown as median and interquartile range (IQR) or as mean ± standard error (SEM).

Summarized data are either shown in boxplots as median ± IQR and mean values included as dashed lines in addition or in bar graphs as mean ± SEM. Normality was tested using the Shapiro-Wilk Test. Normally distributed data were compared with the t-test (two groups) or an ANOVA (more than two groups). Non-normally distributed or small samples of data were compared with the Mann-Whitney-U rank sum test (MWU; two groups) or an ANOVA on ranks (more than two groups). To compare pre- and post-treatment data the paired t-test or the Wilcoxon signed rank test (WSR) was used, depending on the distribution of the data. All statistical tests were two-tailed. P values are indicated as $^{*}P<0.05$, $^{**}P< 0.01$ and $^{***}P<0.001$. The number of experiments n represents the number of cell pairs or cells and was chosen sufficiently high to permit reliable statistical analysis. All of the statistical details of experiments can be found in the figures and corresponding figure legends. Statistics were performed with Sigma Plot 11.0 (Dundas Software) and Mathematica 14.

Acknowledgements

We thank Gudrun Bethge for technical assistance.

This work was supported by a grant of the German research foundation (DFG SCHM1838/6-1 to HS).

Data availability

All data are available in the main text or in the supplemental information and will be shared by the corresponding author upon request. All original code has been deposited at Github and is publicly available as of the date of publication.

Additional information

Author contributions

Conceptualization: H.S., G.B.; Funding acquisition: H.S.; Methodology: all authors; Investigation: M.S., G.B., A.B., A.A., S.B., H.S.; Data Analysis: M.S., G.B., A.B., A.A., S.B., H.S.; Visualization: M.S., G.B., A.B.; Resources: H.S.; Modeling: H.S.; Supervision: H.S.; Writing – original draft: H.S., G.B.; Writing – review & editing: all authors.

Funding

Funder	Grant reference number	Author
Deutsche Forschungsgemeinschaft (DFG)	SCHM1838/6-1	Hartmut Schmidt

Author ORCID iDs

Grit Bornschein: https://orcid.org/0000-0002-4871-2686
Simone Brachtendorf: https://orcid.org/0009-0002-9866-2485
Hartmut Schmidt: https://orcid.org/0000-0002-9516-423X

Additional files

Supplemental information. Figures S1–S4, Table S1 and Supplemental references.

References

Baur D, Bornschein G, Althof D, Watanabe M, Kulik A, Eilers J, Schmidt H (2015) Developmental tightening of cerebellar cortical synaptic influx-release coupling. *J Neurosci* **35**:1858-1871 https://doi.org/10.1523/jneurosci.2900-14.2015 | PubMed

Bornschein G, Schmidt H (2019) Synaptotagmin Ca^{2+} sensors and their spatial coupling to presynaptic Ca_V channels in central cortical synapses. *Front Mol Neurosci* **11**:494 https://doi.org/10.3389/fnmol.2018.00494 | PubMed

Bornschein G, Eilers J, Schmidt H (2019a) Neocortical high probability release sites are formed by distinct Ca^{2+} channel-to-release sensor topographies during development. *Cell Rep* **28**:1410-1418 e1414 https://doi.org/10.1016/j.celrep.2019.07.008 | PubMed

Bornschein G, Brachtendorf S, Schmidt H (2019b) Developmental increase of neocortical presynaptic efficacy via maturation of vesicle replenishment. *Front Synaptic Neurosci* **11**:36 https://doi.org/10.3389/fnsyn.2019.00036 | PubMed

Bornschein G, Brachtendorf S, Reinert A, Eshra A, Kraft R, Hirrlinger J, Eilers J, Hallermann S, Schmidt H (2025) The intracellular Ca^{2+} sensitivity of transmitter release in glutamatergic neocortical boutons. *Science* **389**:48-52 https://doi.org/10.1126/science.adp0870 | PubMed

Borst JG, Helmchen F, Sakmann B (1995) Pre- and postsynaptic whole-cell recordings in the medial nucleus of the trapezoid body of the rat. *J Physiol* **489**:825-840 https://doi.org/10.1113/jphysiol.1995.sp021095 | PubMed

Brachtendorf S, Bornschein G, Schmidt H (2025) Estimates of quantal synaptic parameters in light of more complex vesicle pool models. *Front Cell Neurosci* **19**:1556360 https://doi.org/10.3389/fncel.2025.1556360 | PubMed

Bucurenciu I, Kulik A, Schwaller B, Frotscher M, Jonas P (2008) Nanodomain coupling between Ca^{2+} channels and Ca^{2+} sensors promotes fast and efficient transmitter release at a cortical GABAergic synapse. *Neuron* **57**:536-545 https://doi.org/10.1016/j.neuron.2007.12.026 | PubMed

Bullmann T, Kaas T, Ritzau-Jost A, Wohner A, Kirmann T, Rizalar FS, Holzer M, Nerlich J, Puchkov D, Geis C, *et al.* (2024) Human iPSC-Derived Neurons with Reliable Synapses and Large Presynaptic Action Potentials. *J Neurosci* **44** https://doi.org/10.1523/jneurosci.0971-23.2024 | PubMed

Castillo PE (2012) Presynaptic LTP and LTD of excitatory and inhibitory synapses. *Cold Spring Harbor perspectives in biology* **4**:a005728 https://doi.org/10.1101/cshperspect.a005728 | PubMed

Chanda S, Xu-Friedman MA (2010) A low-affinity antagonist reveals saturation and desensitization in mature synapses in the auditory brain stem. *J Neurophysiol* **103**:1915-1926 https://doi.org/10.1152/jn.00751.2009 | PubMed

Chen JJ, Kaufmann WA, Chen C, Arai I, Kim O, Shigemoto R, Jonas P (2024) Developmental transformation of Ca^{2+} channel-vesicle nanotopography at a central GABAergic synapse. *Neuron* **112**:755-771.e9 https://doi.org/10.1016/j.neuron.2023.12.002 | PubMed

Clements JD, Silver RA (2000) Unveiling synaptic plasticity: a new graphical and analytical approach. *Trends Neurosci* **23**:105-113 https://doi.org/10.1016/s0166-2236(99)01520-9 | PubMed

Douglas RJ, Martin KAC (2004) Neuronal corcuits of the neocortex. *Annual Review of Neuroscience* **27**:419-451 https://doi.org/10.1146/annurev.neuro.27.070203.144152

Doussau F, Schmidt H, Dorgans K, Valera AM, Poulain B, Isope P (2017) Frequency-dependent mobilization of heterogeneous pools of synaptic vesicles shapes presynaptic plasticity. *eLife* **6**:e28935 https://doi.org/10.7554/eLife.28935 | PubMed

Eggermann E, Bucurenciu I, Goswami SP, Jonas P (2012) Nanodomain coupling between Ca^{2+} channels and sensors of exocytosis at fast mammalian synapses. *Nat Rev Neurosci* **13**:7-21 https://doi.org/10.1038/nrn3125 | PubMed

Fedchyshyn MJ, Wang LY (2005) Developmental transformation of the release modality at the calyx of Held synapse. *J Neurosci* **25**:4131-4140 https://doi.org/10.1523/jneurosci.0350-05.2005 | PubMed

Feldman DE (2009) Synaptic mechanisms for plasticity in neocortex. *Annu Rev Neurosci* **32**:33-55 https://doi.org/10.1146/annurev.neuro.051508.135516 | PubMed

Feldman DE (2012) The spike-timing dependence of plasticity. *Neuron* **75**:556-571 https://doi.org/10.1016/j.neuron.2012.08.001 | PubMed

Harris KD, Shepherd GM (2015) The neocortical circuit: themes and variations. *Nat Neurosci* **18**:170-181 https://doi.org/10.1038/nn.3917 | PubMed

Hefft S, Kraushaar U, Geiger JR, Jonas P (2002) Presynaptic short-term depression is maintained during regulation of transmitter release at a GABAergic synapse in rat hippocampus. *J Physiol* **539**:201-208 https://doi.org/10.1113/jphysiol.2001.013455 | PubMed

Helmchen F, Tank DW (2005) A single-compartment model of calcium dynamics in nerve terminals and dendrites. In: Yuste R, Konnerth A (Eds). *Imaging neurons: a laboratory manual* New York: Cold Spring Harbor Laboratory Press. pp. 265-275

Helmchen F, Imoto K, Sakmann B (1996) Ca^{2+} buffering and action potential-evoked Ca^{2+} signaling in dendrites of pyramidal neurones. *Biophys J* **70**:1069-1081 https://doi.org/10.1016/s0006-3495(96)79653-4

Iwasaki S, Takahashi T (2001) Developmental regulation of transmitter release at the calyx of Held in rat auditory brainstem. *J Physiol* **534**:861-871 https://doi.org/10.1111/j.1469-7793.2001.00861.x | PubMed

Koike-Tani M, Kanda T, Saitoh N, Yamashita T, Takahashi T (2008) Involvement of AMPA receptor desensitization in short-term synaptic depression at the calyx of Held in developing rats. *J Physiol* **586**:2263-2275 https://doi.org/10.1113/jphysiol.2007.142547 | PubMed

Kusch V, Bornschein G, Loreth D, Bank J, Jordan J, Baur D, Watanabe M, Kulik A, Heckmann M, Eilers J, *et al.* (2018) Munc13-3 is required for the developmental localization of Ca^{2+} channels to active zones and the nanopositioning of $Ca_V2.1$ near release sensors. *Cell Rep* **22**:1965-1973 https://doi.org/10.1016/j.celrep.2018.02.010 | PubMed

Li L, Bischofberger J, Jonas P (2007) Differential gating and recruitment of P/Q-, N-, and R-type Ca^{2+} channels in hippocampal mossy fiber boutons. *J Neurosci* **27**:13420-13429 https://doi.org/10.1523/jneurosci.1709-07.2007 | PubMed

Lin K-H, Taschenberger H, Neher E (2022) A sequential two-step priming scheme reproduces diversity in synaptic strength and short-term plasticity. *Proceedings of the National Academy of Sciences* **119**:e2207987119 https://doi.org/10.1073/pnas.2207987119 | PubMed

Meyer AC, Neher E, Schneggenburger R (2001) Estimation of quantal size and number of functional active zones at the calyx of held synapse by nonstationary EPSC variance analysis. *J Neurosci* **21**:7889-7900 https://doi.org/10.1523/jneurosci.21-20-07889.2001 | PubMed

Miki T, Malagon G, Pulido C, Llano I, Neher E, Marty A (2016) Actin- and myosin-dependent vesicle loading of presynaptic docking sites prior to exocytosis. *Neuron* **91**:808-823 https://doi.org/10.1016/j.neuron.2016.07.033 | PubMed

Nakamura Y, Harada H, Kamasawa N, Matsui K, Rothman Jason S, Shigemoto R, Silver RA, DiGregorio David A, Takahashi T (2015) Nanoscale distribution of presynaptic Ca^{2+} channels and its impact on vesicular release during development. *Neuron* **85**:145-158 https://doi.org/10.1016/j.neuron.2014.11.019 | PubMed

Narayanan NS, Hyman JM, Seamans J, Rich EL (2025) Computational Properties of the Prefrontal Cortex. *The Journal of Neuroscience* **45**:e1093252025 https://doi.org/10.1523/jneurosci.1093-25.2025 | PubMed

Neher E (2023) Interpretation of presynaptic phenotypes of synaptic plasticity in terms of a two-step priming process. *Journal of General Physiology* **156** https://doi.org/10.1085/jgp.202313454 | PubMed

Neher E, Sakaba T (2001) Combining deconvolution and noise analysis for the estimation of transmitter release rates at the calyx of held. *J Neurosci* **21**:444-461 https://doi.org/10.1523/jneurosci.21-02-00444.2001 | PubMed

Neher E, Brose N (2018) Dynamically primed synaptic vesicle states: Key to understand synaptic short-term plasticity. *Neuron* **100**:1283-1291 https://doi.org/10.1016/j.neuron.2018.11.024 | PubMed

Ohana O, Sakmann B (1998) Transmitter release modulation in nerve terminals of rat neocortical pyramidal cells by intracellular calcium buffers. *J Physiol* **513**:135-148 https://doi.org/10.1111/j.1469-7793.1998.135by.x | PubMed

Regehr WG, Carey MR, Best AR (2009) Activity-dependent regulation of synapses by retrograde messengers. *Neuron* **63**:154-170 https://doi.org/10.1016/j.neuron.2009.06.021 | PubMed

Rozov A, Burnashev N, Sakmann B, Neher E (2001) Transmitter release modulation by intracellular Ca^{2+} buffers in facilitating and depressing nerve terminals of pyramidal cells in layer 2/3 of the rat neocortex indicates a target cell-specific difference in presynaptic calcium dynamics. *J Physiol* **531**:807-826 https://doi.org/10.1111/j.1469-7793.2001.0807h.x | PubMed

Sabatini BL, Oertner TG, Svoboda K (2002) The life cycle of Ca^{2+} ions in dendritic spines. *Neuron* **33**:439-452 https://doi.org/10.1016/s0896-6273(02)00573-1 | PubMed

Scheuss V, Schneggenburger R, Neher E (2002) Separation of presynaptic and postsynaptic contributions to depression by covariance analysis of successive EPSCs at the calyx of held synapse. *J Neurosci* **22**:728-739 https://doi.org/10.1523/jneurosci.22-03-00728.2002 | PubMed

Schmidt H (2019) Control of presynaptic parallel fiber efficacy by activity-dependent regulation of the number of occupied release sites. *Frontiers in systems neuroscience* **13**:30 https://doi.org/10.3389/fnsys.2019.00030 | PubMed

Schmidt H, Stiefel K, Racay P, Schwaller B, Eilers J (2003) Mutational analysis of dendritic Ca^{2+} kinetics in rodent Purkinje cells: role of parvalbumin and calbindin D_{28k}. *J Physiol (Lond)* **551**:13-32 https://doi.org/10.1113/jphysiol.2002.035824 | PubMed

Schmidt H, Brachtendorf S, Arendt O, Hallermann S, Ishiyama S, Bornschein G, Gall D, Schiffmann SN, Heckmann M, Eilers J (2013) Nanodomain coupling at an excitatory cortical synapse. *Curr Biol* **23**:244-249 https://doi.org/10.1016/j.cub.2012.12.007 | PubMed

Scimemi A, Diamond JS (2012) The number and organization of Ca^{2+} channels in the active zone shapes neurotransmitter release from Schaffer collateral synapses. *J Neurosci* **32**:18157-18176 https://doi.org/10.1523/jneurosci.3827-12.2012 | PubMed

Silver RA (2003) Estimation of nonuniform quantal parameters with multiple-probability fluctuation analysis: theory, application and limitations. *J Neurosci Methods* **130**:127-141 https://doi.org/10.1016/j.jneumeth.2003.09.030 | PubMed

Taschenberger H, Leao RM, Rowland KC, Spirou GA, von Gersdorff H (2002) Optimizing synaptic architecture and efficiency for high-frequency transmission. *Neuron* **36**:1127-1143 https://doi.org/10.1016/s0896-6273(02)01137-6 | PubMed

Tran V, Stricker C (2018) Diffusion of Ca^{2+} from small boutons en passant into the axon shapes AP-evoked Ca^{2+} transients. *Biophys J* **115**:1344-1356 https://doi.org/10.1016/j.bpj.2018.07.018 | PubMed

Vyleta NP, Jonas P (2014) Loose coupling between Ca^{2+} channels and release sensors at a plastic hippocampal synapse. *Science* **343**:665-670 https://doi.org/10.1126/science.1244811 | PubMed

Weichard I, Taschenberger H, Gsell F, Bornschein G, Ritzau-Jost A, Schmidt H, Kittel RJ, Eilers J, Neher E, Hallermann S, *et al.* (2023) Fully-primed slowly-recovering vesicles mediate presynaptic LTP at neocortical neurons. *Proc Natl Acad Sci U S A* **120**:e2305460120 https://doi.org/10.1073/pnas.2305460120 | PubMed

Peer reviews

Reviewer #1 (Public review):

Summary:

This study asks whether synapses formed by the same broad neuronal class (excitatory pyramidal neurons, PN) adapt their presynaptic organization in a cortex-specific manner, comparing the prefrontal cortex (PFC) with the primary somatosensory cortex (S1). The authors combine sophisticated electrophysiology (paired recordings and extracellular minimal stimulation), pharmacological perturbations of presynaptic Ca^{2+}-secretion coupling, bouton Ca^{2+} imaging, and mechanistic modeling. Across two prominent excitatory connections (Layer 5 (L5) PN-L5PN and L2/3-L5PN), they provide convergent evidence that mature PFC synapses operate with looser Ca^{2+} channel-release sensor coupling than their S1 counterparts.

Overall, the study provides an appealing mechanistic link between synaptic nano/micro-architecture and cortical-area specialization. The idea that PFC synapses retain a more "plasticity-favoring" presynaptic state, while the primary sensory cortex emphasizes reliability and timing precision, is potentially impactful for how we think about circuit computation and plasticity across cortical hierarchies.

Strengths:

A major strength is the multi-pronged experimental strategy. The paper first establishes robust, area-dependent differences in synaptic efficacy, reliability, timing, and short-term plasticity (facilitation prevailing in PFC versus depression in S1), using both paired recordings and minimal extracellular stimulation paradigms. The coupling interpretation is then directly supported by differential sensitivity to EGTA (and appropriate positive-control effects of fast chelators). Finally, volume-averaged calcium signals are reported to be similar across areas, arguing against trivial explanations based on gross differences in calcium influx, and the modeling provides a quantitative framework for interpreting the observed chelator effects.

Weaknesses:

Limitations are minor and concern interpretation/clarity rather than core results. Some key inferences rely on indirect readouts (chelator sensitivity, fluctuation analysis-derived parameters, bouton-averaged calcium signals), each of which carries assumptions and potential confounds that should be discussed more explicitly. In particular, the repatching paradigm for the paired-recording EGTA experiment, though very impressive, and the limited number of extracellular calcium conditions used for fluctuation analysis (three concentrations), can influence quantitative estimates and the confidence intervals around them.

https://doi.org/10.7554/eLife.110314.1.sa3

Reviewer #2 (Public review):

Schwarze et al. investigated whether synaptic efficacy is brain-region specific. To this end, they compared synaptic connections established by layer 5 (L5) neocortical pyramidal cells and between L5 and L2/3 pyramidal cells. In order to identify the mechanism of this brain region specificity, the authors employed several experimental approaches, including paired electrophysiological recordings, extracellular stimulation, low- and high-affinity intracellular calcium chelators (EGTA and BAPTA), multiple probability fluctuation analysis (MPFA), and intracellular measurements of calcium transients as well as computational modelling. The findings of the present study indicate that synaptic connections in the primary somatosensory cortex (S1) are significantly stronger and more reliable than those in the prefrontal cortex (PFC).

The study is timely, and the topic is of significant interest to the neuroscience community. Despite the extensive research that has been carried out on the neuroanatomy and receptor distribution of different brain regions, comparatively little attention has been paid to differences in synaptic physiology. The authors' approach is characterised by its elegance and comprehensive nature, and the conclusions drawn are compelling. Nevertheless, there are a number of unresolved issues.

Major points:

(1) The authors state that data from the S1 cortex were obtained in a previous study. In the context of an explicitly comparative study (PFC vs. S1cortex), it would have been advantageous for the authors to perform a subset of experiments in which both cortices were obtained from a single animal. This is a feasible undertaking, given the spatial separation of the PFC and S1 cortex.

(2) Figure 1A is somewhat misleading because it could suggest that the authors have performed dual recordings in identified PFC pyramidal cells.

(3) PFC and S1 cortex in rodents differ markedly in their morphological organisation. For example, in all sensory cortices, layer 4 is very pronounced; however, in the PFC of rodent,s no clear layer 4 can be found. On the other hand, PFC shows a clear separation of layers 2 and

3, which is not visible inthe S1 cortex. Furthermore, PFC pyramidal cells in layers 2, 3, and 5 exhibit significant heterogeneity, diverging considerably from those found in layers 5a and 5b of S1 cortex. Thus, there is no clear correlation between L5 pyramidal cells in the PFC and the S1 cortex. In order to achieve a meaningful comparison of the data obtained in PFC and S1 cortex, it is necessary for the authors to determine whether the record is from similar pyramidal cell populations.

(3) In addition, PFC pyramidal cells in layer 2, 3 and 5 are highly heterogeneous and differ markedly from those in layer 5a and 5b of S1 cortex. To achieve a meaningful comparison of the data obtained in the PFC and the S1 cortex, the authors need to determine whether the record from similar pyramidal cell populations.

(4) For the S1 cortex, in rats it has been found that L5 synaptic connection between pairs of L5a pyramidal cells and pairs of L5b pyramidal cells differ markedly with respect to mean EPSP amplitude, latency and coefficient of variation (cv, a surrogate measure for the synaptic release probability) (cf. Markram et al., 1997; Frick et al., 2008). It is therefore likely that PFC and S1 pre- and postsynaptic pyramidal cells are not only morphologically and electrophysiological distinct but also with respect to their synaptic properties. At least, the authors need to discuss these confounding issues and preferentially address them experimentally. For example, it would be helpful to demonstrate that paired recordings were made from the same pyramidal cell types, perhaps by documenting their morphology and/or firing patterns. In addition, they should discuss the marked difference in EPSP amplitude and putative release probability between their data and the earlier studies.

(5) In order to perform multiple probability fluctuation analysis (MPFA), a parabolic fit with a mere three points is inadequate, particularly because 2 mM and 5 mM Ca2+ are close to the peak of the variance-to-mean parabola, and only 1 mM Ca2+ is on its initial linear part. A more meaningful result would have been obtained with an additional Ca2+ concentration between 1.0 and 2.0 mM, as these are closer to the physiological range. In this context, the authors should have quoted the more recent and more detailed paper by the Silver group (Saviane and Silver, 2006; Lanore and Silver, 2016) and not just the Clements and Silver review paper.

(6) Methods: The authors should clarify whether their paired recordings from L5 pyramidal cells involved whole-cell recordings from both pre- and postsynaptic neurons. From Figure 1B, it appears as if the presynaptic neurons were not recorded in whole cell mode but rather stimulated in cell-attached mode. This is also reflected in the artefact visible in the current trace recorded in the postsynaptic neuron. The authors should explicitly state their methodological approach and mention how reliable the timing of the presynaptic action potential was under these circumstances. The same holds true for the extracellular stimulation protocol. A significantly more detailed description of the experimental protocol is necessary here.

(7) Methods: The authors use Student's t-test for data comparison. The authors should verify that the data distribution was indeed normal, e.g. by using a Shapiro-Wilk test. If this is not the case, non-parametric tests should be used.

https://doi.org/10.7554/eLife.110314.1.sa2

Reviewer #3 (Public review):

Summary:

In this manuscript, Max Schwarze and colleagues examined the coupling distance between presynaptic Ca^{2+} channels and the vesicular release sensor at neocortical synapses in mice. They propose that Ca^{2+} channel-release sensor coupling differs across cortical areas, with

relatively loose (microdomain) coupling in prefrontal cortex (PFC) and tighter (nanodomain) coupling in primary somatosensory cortex (S1) for comparable pyramidal-neuron synapse types. To test this, they combine paired recordings and minimal stimulation with chelator manipulations (EGTA/BAPTA), mean-variance/MPFA-style analyses, presynaptic Ca^{2+} imaging, and computational modeling. They conclude that presynaptic coupling organization is area-specific in the mature cortex and contributes to regional differences in synaptic timing, reliability, and short-term plasticity.

Strengths:

This study tackles an important question and is strengthened by a cohesive body of evidence assembled from multiple complementary approaches. A major asset is the inclusion of high-value datasets, particularly the paired recordings between L5 pyramidal neurons and the systematic assessment of EGTA sensitivity, which provide a solid functional foundation for the authors' central claims. The work is further distinguished by its genuinely multimodal design: combining electrophysiology with presynaptic calcium imaging (and integrating these observations with quantitative analyses and modeling) offers a more mechanistic view of neurotransmitter release than any single method could provide. Overall, the direct, within-framework comparison of presynaptic release-control mechanisms across cortical areas for comparable synapse types is compelling and gives the conclusions a level of robustness and interpretability that is often difficult to achieve in studies of cortical synaptic diversity.

Weaknesses:

Several aspects would benefit from clearer explanation, stronger integration with the existing literature, and a more explicit discussion of limitations and potential confounds. Without these additions, some conclusions remain speculative. Throughout the manuscript, the authors also often imply that different measurements reflect the same underlying synapse population. This is unlikely to be strictly true across all experiments and makes it difficult to integrate results from the various approaches into a single, unified set of functional synaptic properties. In addition, some statements-particularly those linking coupling mode to "higher-order neocortical functions"-appear broader than what is directly supported by the experiments and should be tempered or more precisely scoped.

Below, I list several topics that could help better frame the main findings of the present study and clarify how it relates to previously published work.

(1) The authors use EGTA sensitivity of EPSCs (together with additional metrics) to argue that S1 and PFC synapses differ in Ca^{2+} channel-release sensor coupling. While this is a plausible interpretation, EGTA effects are not uniquely determined by coupling distance and can also reflect differences in Ca^{2+} entry kinetics, action potential waveform, endogenous buffering/extrusion, or release-sensor/vesicle state. The authors use a constrained modeling approach, but the rationale for the different constraint sets is not fully clear from the current description. It would be helpful to expand and clarify the Methods section to explain how these constraints were defined, justified, and applied (and how alternative constraint choices would affect the results). In this context, the Abstract's broader claim that the study "reveals microdomain coupling as a presynaptic structure-function correlate of higher-order neocortical functions" appears overstated. Given the well-known diversity of cortical synapses even within a single region (e.g., synapses onto different interneuron subclasses or different PN cell types, extracortical sources like thalamus), the authors should clarify the intended scope: is the conclusion meant to apply broadly across synapse classes in S1 and PFC, or only to the specific connection type(s) examined here?

(2) The chelator logic is sound in principle, but the Discussion should more explicitly acknowledge standard caveats and alternative explanations. The authors partly address this by including presynaptic Ca^{2+} imaging and modeling, yet it would help to explain more

clearly how the combination of (i) chelator sensitivity, (ii) presynaptic Ca^{2+} signals, and (iii) model constraints rules out-or substantially reduces the likelihood of-changes in AP waveform, Ca^{2+} influx kinetics, buffering/extrusion, or sensor/vesicle state as the primary drivers. In addition, recent hypotheses emphasizing vesicle priming and/or release-site occupancy as contributors to apparent EGTA sensitivity should be discussed as a complementary or alternative interpretation.

(3) A substantial portion of the S1 comparison appears to rely on previously published datasets. This should be made unambiguous in the Results and Methods, and it would be helpful to summarize this clearly (e.g., in a table indicating which figures/analyses use new data versus reanalysis of published data). If this information is already present, it should be highlighted more prominently.

(4) The modeling is informative, but the choice of a specific VGCC-release-site geometry and channel arrangement is not sufficiently justified. The manuscript adopts a particular spatial configuration, yet the rationale for selecting this geometry, rather than other plausible architectures discussed in the literature, is not clearly explained, nor is it meaningfully revisited in the Discussion. The authors should justify why the same organization is assumed across two distinct cortical areas and, ideally, include (or at a minimum discuss) a sensitivity analysis showing how key inferences (e.g., coupling distance and channel number) depend on the assumed geometry.

(5) The calcium imaging data are valuable, but given the diversity of synapses within each cortical layer, it is not clear that imaged boutons can be confidently assigned to the specific connection types being interrogated electrophysiologically. A substantial fraction of boutons likely corresponds to different postsynaptic targets (including interneurons and distinct pyramidal-cell classes), and this heterogeneity could complicate interpretation. This limitation should be discussed explicitly

(6) In unitary connections, the authors assess EGTA effects alongside other functional parameters (strength, delay, short-term plasticity), which is a major strength. However, for L2/3 to L5 connections, it appears that EGTA sensitivity was tested primarily using extracellular stimulation. Given anatomical and circuit differences between PFC and S1, extracellular stimulation may recruit different synapse populations across regions, potentially confounding regional comparisons of EGTA sensitivity. This limitation should be acknowledged explicitly. While I am not requesting technically demanding L2/3↔L5 paired recordings in S1, the possibility that different synapse identities are being sampled should be treated as a meaningful source of uncertainty. The Discussion would also benefit from placing the magnitude of EGTA effects in the context of prior "loose coupling" literature, where comparatively large EGTA effects have been reported in some systems. In addition, the reported difference between adult PFC EGTA effects and S1 inhibition appears small (on the order of <10%) and should be interpreted cautiously, especially given that PFC and S1 mature on different timelines and P21-P26 is unlikely to reflect a mature PFC circuit state. The adult cohort (P90-P100) is therefore important, but the age mismatch complicates PFC-S1 comparisons; ideally, S1 should be assessed at matched ages, or this limitation should be discussed explicitly. Finally, for statistical robustness, in panel D of Figure 2, were the comparisons corrected for multiple testing to control Type I error?

(7) Alterations in initial release probability are often associated with changes in short-term plasticity. In the present manuscript, the authors report similar initial release probability at PFC and S1 synapses, yet observe differences in short-term plasticity profiles. The mechanistic basis for this apparent dissociation is not addressed and should be discussed explicitly, including potential explanations.

(8) There are multiple instances where the text appears to cite non-existent or misnumbered figure panels (e.g., references to "Figure 4G-I / 4J" when the relevant material appears

elsewhere). These should be corrected throughout, as they currently reduce readability and confidence.

(9) The Methods describe P21-P26 animals, whereas the Results include older cohorts (e.g., P90-P100) and additional regions (e.g., mPFC). The Methods should be updated so that all cohorts and regions analyzed in the Results are fully described.

https://doi.org/10.7554/eLife.110314.1.sa1

Author response:

We will extend and clarify the text of the paper according to the suggestions of the reviewers. In particular we will extend the description and discussion of the calcium chelator approach, re-patching and multiple probability fluctuation analysis. We will also include in the Results section that volume-averaged calcium signals were measured and extend the description about measurement of the resting calcium and variability between boutons. Literature will be included and discussed as suggested.

In order to avoid any misunderstandings, we will also make it clearer that recordings from

L5PN – L5PN synapses in S1 were published in our preceding papers (Bornschein et al., 2019a, b), but that these data were partially reanalyzed for the comparison with recordings from L5PN – L5PN synapses in PFC (this paper). We will also emphasize that the recordings from L2/3 to L5PN synapses in S1 and PFC were made directly in the present study. We will include a supplementary table, which explicitly shows for each figure which data are from Bornschein et al. (2019a, b) and which data were obtained in the present study.

We will consider all points of the reviewers and the recommendations of the editors in detail in the revised manuscript and/or our pointwise response.

We recognized one factual error in the public reviews:

Reviewer 2, point 7: “Methods: The authors use Student's t-test for data comparison. The authors should verify that the data distribution was indeed normal, e.g. by using a Shapiro-Wilk test. If this is not the case, non-parametric tests should be used.”

A detailed description of the statistics, including test for normality, is given in the Methods section. In particular we wrote in the Methods: “Normality was tested using the Shapiro-Wilk Test. (…) To compare pre- and post-treatment data the paired t-test or the Wilcoxon signed rank test (WSR) was used, depending on the distribution of the data. (…)”

To further emphasize that the data was tested for normal distribution, we have also extended the description of the statistical tests in the figure legends.

Bornschein G, Brachtendorf S, Schmidt H (2019a) Developmental increase of neocortical presynaptic efficacy via maturation of vesicle replenishment. Front Synaptic Neurosci 11:36.

Bornschein G, Eilers J, Schmidt H (2019b) Neocortical high probability release sites are formed by distinct Ca2+ channel-to-release sensor topographies during development. Cell Rep 28:1410-1418 e1414.

https://doi.org/10.7554/eLife.110314.1.sa0